

Atomic structure of [0001]-tilt grain boundaries in ZnO: A high-resolution TEM study of fiber-textured thin films

Fumiyasu Oba,^{1,*} Hiromichi Ohta,² Yukio Sato,³ Hideo Hosono,^{2,4} Takahisa Yamamoto,³ and Yuichi Ikuhara^{1,†}

¹*Institute of Engineering Innovation, The University of Tokyo, 2-11-16 Yayoi, Bunkyo-ku, Tokyo 113-8656, Japan*

²*Transparent ElectroActive Materials Project, ERATO, Japan Science and Technology Agency, 3-2-1 Sakado, Takatsu-ku, Kawasaki 213-0012, Japan*

³*Department of Advanced Materials Science, The University of Tokyo, 7-3-1 Hongo, Bunkyo-ku, Tokyo 113-8656, Japan*

⁴*Materials and Structures Laboratory, Tokyo Institute of Technology, 4259 Nagatsuta, Midori-ku, Yokohama 226-8503, Japan*

(Received 12 February 2004; published 20 September 2004)

The atomic structure of [0001]-tilt grain boundaries in ZnO was investigated using high-resolution transmission electron microscopy (HRTEM) and atomistic calculations. HRTEM observation was conducted for [0001] fiber-textured ZnO thin films grown on quartz-glass substrates by the pulsed-laser deposition. The [0001]-tilt boundaries observed in the films can be classified into three types: low-angle boundaries composed of irregular dislocation arrays, boundaries with $\{10\bar{1}0\}$ facet structures, and near-low Σ boundaries represented by symmetric periodicity units. The atomic structure of the boundaries is discussed with a focus on a $\Sigma=7$ boundary in conjunction with atomistic calculations and HRTEM image simulations. The $\Sigma=7$ boundary consists of multiple structural units that are very similar to the core structures of edge dislocations. Straight or zigzag arrangements of the dislocationlike structural units constitute other high-angle boundaries with symmetric and $\{10\bar{1}0\}$ facet structures as well. It is suggested that [0001]-tilt boundaries in ZnO are generally described as an array of the dislocationlike units.

DOI: 10.1103/PhysRevB.70.125415

PACS number(s): 68.35.-p, 68.37.Lp

I. INTRODUCTION

It is recognized that the macroscopic properties of polycrystalline materials are often determined by the atomic and electronic structure of grain boundaries. The importance has stimulated experimental and theoretical investigations in the past decades. High-resolution transmission electron microscopy (HRTEM) and scanning TEM (STEM) are known as powerful experimental techniques to reveal the atomic structure of grain boundaries.¹⁻⁶ In combination with electron energy-loss spectroscopy, it is also possible to access the electronic structure even with an atomistic spatial resolution.^{5,6} Theoretical calculations based on empirical and first-principles methods have been employed for the modeling of grain boundaries as well.⁷⁻¹⁶ However, these experimental and theoretical approaches have been applied mostly to special grain boundaries with relatively simple geometries. The systematic understanding of interfacial atomic-electronic structure is still lacking, especially for metal oxides. This is partly due to the limitation in HR-TEM and -STEM observation; the number of grain boundaries that are accessible on an atomistic scale is usually limited in polycrystalline materials.

An effective way to study the atomic structure of grain boundaries is the use of bicrystals, in which grain boundaries with aimed misorientations are fabricated by the diffusion bonding of two single crystals. There are a number of reports on interfacial atomic structure in metal oxide bicrystals.^{3,5,6,17-27} Another type of specimen suited to this objective would be fiber-textured materials. Since tilt grain boundaries with a common rotation axis can be dominantly present because of the fiber-texture, HR-TEM and -STEM observation would be applicable to most of the boundaries. It

is even possible to gather systematic information on tilt grain boundaries from one specimen. HRTEM observations of tilt boundaries in fiber-textured ZrO_2 and GaN have been performed to reveal their atomic structures.^{28,29} In particular, Potin *et al.* have conducted an extensive HRTEM study of [0001] grain boundaries in GaN films, and systematically discussed the atomic structure in comparison with that of edge dislocations.²⁹

Among metal oxides, ZnO exhibits one of the most interesting phenomena associated with grain boundaries. In a doped polycrystalline form, it shows highly nonlinear current-voltage characteristics that are suited to applications as varistors.³⁰⁻³² These characteristics are attributed to the electrostatic potential barriers formed at grain boundaries and strongly depend on the geometry and chemical composition of boundaries, as well as the microstructure.³³⁻³⁷ Recent studies on the electrical properties of single grain boundaries in ZnO bicrystals indicate that the disorder in atomic arrangement does not essentially affect the properties, and dopants and native defects segregated at boundaries play primary roles.³⁸⁻⁴¹ Still, it is important to understand the atomic structure since it mainly determines the dopant-native defect segregation behavior. For basal inversion boundaries, the relationship between atomic structure and dopant segregation has been investigated in detail using HRTEM and x-ray energy-dispersive spectroscopy.^{42,43} ZnO has also attracted increasing interest because of the transparent conducting and ultraviolet light-emitting properties.⁴⁴⁻⁴⁷ In this case, the discontinuity of crystal lattices at grain boundaries mostly degrades the electrical and optical properties. A detailed knowledge on grain boundary atomic structure should be required to understand the deterioration mechanism.

In the present study, [0001] fiber-textured ZnO thin films were fabricated, and many types of tilt grain boundaries

TABLE I. CSL misorientations with $\Sigma < 50$ for grain boundaries with a [0001] rotation axis in the hexagonal system. Boundary planes that provide symmetric tilt grain boundaries (STGBs) are also listed.

Σ value	Rotation angle(degree)	Boundary plane for STGB
7	21.79	$\{1\ 2\ \bar{3}\ 0\}$, $\{1\ 4\ \bar{5}\ 0\}$
13	27.80	$\{2\ 5\ \bar{7}\ 0\}$, $\{1\ 3\ \bar{4}\ 0\}$
19	13.17	$\{2\ 3\ \bar{5}\ 0\}$, $\{1\ 7\ \bar{8}\ 0\}$
31	17.90	$\{4\ 7\ \bar{11}\ 0\}$, $\{1\ 5\ \bar{6}\ 0\}$
37	9.43	$\{3\ 4\ \bar{7}\ 0\}$, $\{1\ 10\ \bar{11}\ 0\}$
43	15.18	$\{5\ 8\ \bar{13}\ 0\}$, $\{1\ 6\ \bar{7}\ 0\}$
49	16.43	$\{3\ 5\ \bar{8}\ 0\}$, $\{2\ 11\ \bar{13}\ 0\}$

therein were investigated by HRTEM in conjunction with atomistic calculations. The atomic structure of the grain boundaries is discussed with a focus on a relationship to edge dislocation core structures.

II. EXPERIMENTAL AND COMPUTATIONAL PROCEDURES

ZnO thin films with a thickness of about 150 nm were grown on quartz-glass substrates by the pulsed-laser deposition. Using a KrF excimer laser beam (wavelength, 248 nm pulse duration, 20 ns repetition frequency, 10 Hz), the deposition was made under a substrate temperature of 400 °C, and an oxygen partial pressure and a back pressure of 1.2×10^{-3} and 1×10^{-6} Pa, respectively. X-ray diffractometry revealed that the thin films have a fiber-textured structure with a common [0001] axis normal to the substrate surfaces. The rocking curve of the (0002) peak showed a full width at half maximum of 2.2°, indicating that most of the grains have (0001) out-of-plane misalignments of less than 1°. Therefore, many of the grain boundaries in the films are expected to be near [0001]-tilt type. To obtain energetically favorable boundaries, the films were annealed at 800 °C for 3 h in air after the deposition.

Plan-view TEM foils were prepared by back thinning the as-deposited and annealed specimens from the substrate side, which includes mechanical grinding and dimpling down to about 20 μm and argon-ion-beam thinning to an electron transparency using DuoMill Model 600 with gun energies of 3–4 keV and a beam angle of 13° (Gatan, Inc., Pleasanton, CA). The TEM observation was conducted on a JEM-4010 operated at 400 kV (JEOL, Tokyo, Japan).

Atomistic calculations and HRTEM image simulations were employed to investigate the atomic structure of one of the boundaries in low Σ coincidence site lattice (CSL) misorientations,⁴⁸ the $\Sigma=7$, $\{12\bar{3}0\}$ boundary, in comparison with HRTEM. As shown in Table I, this boundary has the lowest Σ value among [0001] boundaries in hexagonal system, and the $\{12\bar{3}0\}$ boundary planes give a symmetric periodicity unit with the smallest periodicity. The atomistic calculations were performed using the GULP program code

based on the lattice statics method.⁴⁹ Under three-dimensional periodic boundary conditions, the lattice energy was described as a long-range Madelung potential and short-range Buckingham potentials. The potential parameter set reported by Lewis and Catlow was used,⁵⁰ which has been confirmed to reproduce lattice and elastic constants of ZnO fairly well,¹⁴ and to give boundary atomic configurations very close to those obtained by first-principles calculations.¹⁵ The total energy was iteratively minimized to achieve the optimum atomic positions in simulation cells at 0 K using the quasi-Newton method with the Broyden-Fletcher-Goldfarb-Shanno hessian update scheme.⁵¹ For the calculation of the $\Sigma=7$ boundary, supercells containing two identical boundaries were constructed to match the three-dimensional periodic boundary conditions. To test the convergence of the boundary energy with respect to the distance between the boundaries, two sizes of supercells composed of 180–192 atoms and 292–304 atoms were employed, where the distances are about 2.5 and 4 nm, respectively. The geometry optimization, namely energy minimization, was performed for the supercells of the $\Sigma=7$ boundary in various three-dimensional translation states with an increment of about 0.03 nm. The boundary energy was evaluated as a function of the translation states, and configurations in the local energy minima were selected as equilibrium structures. Calculations were then performed around the local minima with finer translational increments of approximately 0.01 nm in order to refine the obtained structures. These computational procedures are based on two-dimensional lattice static simulations previously conducted for the same $\Sigma=7$ boundary.¹⁴ The structures obtained in the present study are essentially identical with the results of the two-dimensional simulations. In addition, configurations with an atomic column added to or removed from the equilibrium structures were investigated to find other possible equilibrium structures, since these configurations are not equivalent to those obtained through the simple translation.

HRTEM image simulations were conducted for the modeled atomic configurations using the TEMPAS program code (Total Resolution, Berkeley, CA) based on the multislice method.⁵² HRTEM images were systematically calculated as a function of defocus and specimen thickness to search conditions that give the best agreement with an experimental image.

III. RESULTS AND DISCUSSION

A. Microstructure of ZnO thin films

Figure 1 shows plan-view bright-field images and selected-area diffraction patterns taken from as-deposited and annealed ZnO films. It is recognized that the as-deposited film is a polycrystal with a grain size of less than 30 nm. The diffraction pattern shows rings composed of a series of spots, which are particular to polycrystalline materials. The detailed analysis, however, revealed that the spots associated with (000*n*) planes are absent. This indicates that all the grains have [0001] axes nearly parallel to the incident electron beam direction. Therefore, many of the grain boundaries in this film are expected to be tilt type with a [0001]

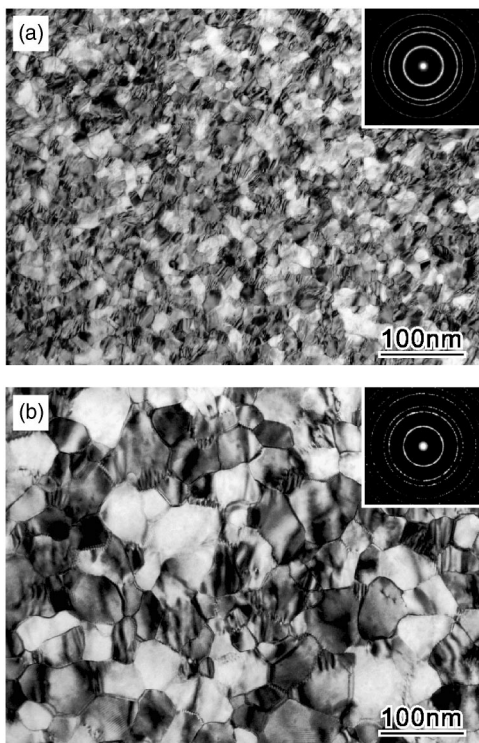


FIG. 1. Plan-view bright-field images and selected-area diffraction patterns taken from ZnO thin films. (a) As deposited. (b) Annealed at 800 °C for 3 h.

rotation axis. The bright-field images shown in Fig. 1 were taken with an incident electron beam direction little off from the [0001] in order to clarify the microstructure. If the zone axis was exactly set at the [0001], all the grains just appeared dark, which supports a good out-of-plane alignment indicated by x-ray diffractometry.

For the annealed film shown in Fig. 1(b), a grain growth has occurred to result in a grain size of 30–100 nm. The diffraction pattern is again ringlike without the spots/rings arising from the (000*n*) planes. The [0001] fiber-textured structure had been preserved during the annealing. In this annealed film, many of boundaries look flat and located parallel to the [0001] axis, at least within a thickness of the TEM foil as recognized in HRTEM images shown later. These features may be attributed to a grain growth to reduce the boundary area, and hence the total boundary energy that is the product of the boundary area and energy per area.

HRTEM observation was conducted for grain boundaries in the annealed film to investigate their atomic structures. Figure 2 displays HRTEM images of typical grain boundaries with different characters in atomic structure. Under the imaging condition employed, the bright spots approximately correspond to the open channels along the [0001] direction in ZnO. The crystal structure is schematically shown in Fig. 3. The open channels represent the edge of the ZnO primitive cell in the wurtzite structure (*P6₃mc*) and have the sixfold symmetry in the [0001] projection, as well as the atomic columns. The distance between the open channels or bright spots in the HRTEM images is equal to the lattice constant *a*, 0.325 nm.⁵³ Because of the sixfold symmetry in the [0001]

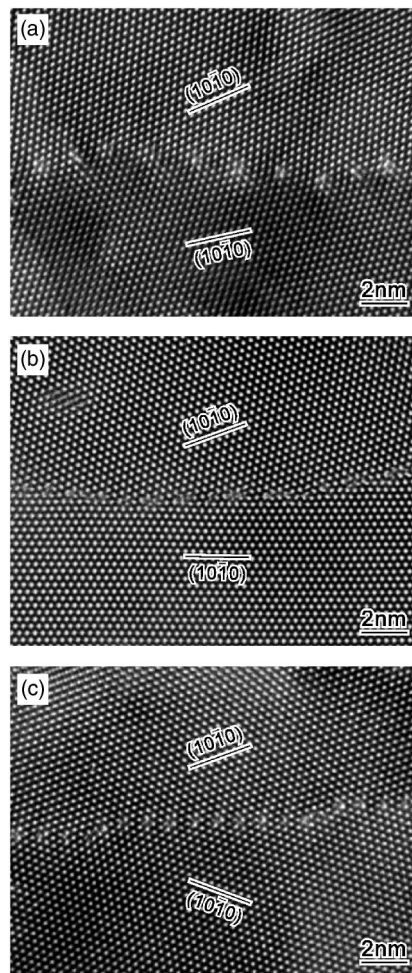


FIG. 2. HRTEM images of typical [0001]-tilt grain boundaries in annealed ZnO thin films. (a) $10.6 \pm 0.1^\circ$ boundary composed of a dislocation array. (b) $20.1 \pm 0.2^\circ$ near $\Sigma=7$ boundary having a $\{10\bar{1}0\}$ facet structure. (c) $20.0 \pm 0.2^\circ$ near $\Sigma=7$ boundary with a symmetric structure.

projection, the rotation angle of [0001]-tilt boundaries ranges between 0° and 30° . Various microscopic geometries are present within respective rotation angles, depending on boundary planes and translation states.⁵⁴

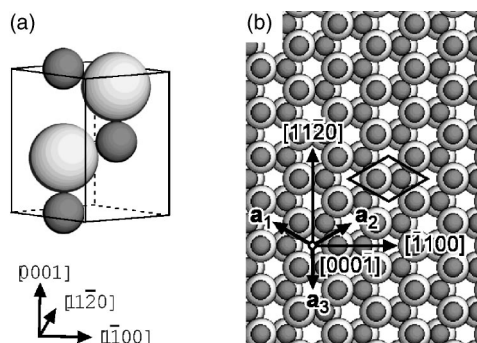


FIG. 3. (a) Schematic of the ZnO primitive cell. The smaller and larger circles denote Zn and O, respectively. (b) View from the [000 $\bar{1}$] direction. \mathbf{a}_1 – \mathbf{a}_3 correspond to three of $1/3\langle 11\bar{2}0 \rangle$ primitive translation vectors. The rhombus indicates the primitive cell.

The boundary shown in Fig. 2(a) has a rotation angle of $10.6 \pm 0.1^\circ$, which was estimated from Fourier transforms of the HRTEM image. An array of strong contrasts is recognized along the boundary. This is due to the presence of edge dislocations with a Burgers vector of $1/3\langle 11\bar{2}0 \rangle$, as will be discussed in the following sections. Such a boundary composed of a dislocation array is often referred to as a low-angle boundary. It is presumed that the misorientation is fully accommodated by dislocations at this type of boundary, and the distance between adjacent dislocations is inversely related to the rotation angle.⁵⁵ An extensive HRTEM observation indicated that the arrays of dislocations have a tendency to be more irregular when boundaries have relatively low rotation angles, i.e., relatively large dislocation intervals. The boundary shown in Fig. 2(a) has a somewhat curved and irregular array of dislocations, but this feature was clearer for boundaries with lower rotation angles. On the other hand, when the rotation angles were relatively large, dislocations mostly showed regular alignments to form nearly flat boundaries. Such a straight arrangement is considered to be favorable in terms of the elastic field associated with dislocations.⁵⁶

Figure 2(b) shows a boundary with a rotation angle of $20.1 \pm 0.2^\circ$. This is composed of two types of flat structures. In the left-hand side of the figure, the boundary is located almost on a $(10\bar{1}0)$ plane of the lower grain to give an asymmetric structure. Moving on to the right-hand side, the boundary is gradually shifted toward the upper grain, and finally has a nearly symmetric structure. Such a symmetric structure is particular to the boundaries with a low Σ CSL misorientation. As recognized in Table I, the rotation angle of this boundary is actually close to that of the $\Sigma=7$, 21.79° , and the symmetric boundary plane is located near one of the $\{14\bar{5}0\}$ planes. Another boundary of this type is presented in Fig. 2(c), where flat and symmetric structures are recognized between two steps. In the figure, the $(10\bar{1}0)$ planes of the upper and lower grains making an angle of 40° are indicated by lines for consistency with the boundaries shown in Figs. 2(a) and 2(b), but the rotation angle actually corresponds to $20.0 \pm 0.2^\circ$. This angle is almost the same as that of the boundary shown in Fig. 2(b), and hence is close to that of the $\Sigma=7$. This boundary is located near one of the $\{12\bar{3}0\}$ planes, the other set of the planes that gives a symmetric structure in the $\Sigma=7$ misorientation. The difference in the boundary plane between the boundaries shown in Figs. 2(b) and 2(c) makes a significant dissimilarity in local atomic structure, as will be shown later.

A comprehensive HRTEM observation of grain boundaries in the annealed ZnO thin film indicated that the $[0001]$ -tilt boundaries therein can be classified into the three types mentioned above: low-angle boundaries that are described as an irregular array of dislocations, boundaries with $\{10\bar{1}0\}$ facet structures, and near-low Σ boundaries composed of symmetric structural units. The detailed atomic structures of these grain boundaries will be discussed in the following sections.

B. Atomic structure of a $\Sigma=7$ boundary

In order to approach the general atomic structure of $[0001]$ -tilt boundaries in ZnO, a $\Sigma=7$ $\{12\bar{3}0\}$ boundary was investigated using atomistic calculations in conjunction with the HRTEM observation. This boundary was selected because boundaries nearly in this misorientation were frequently observed in the present ZnO thin films, and its periodic structure with the smallest periodicity among the $[0001]$ boundaries is suited for a detailed theoretical analysis. As a result of the atomistic calculations, some types of boundary atomic configurations were obtained as equilibrium configurations that correspond to the local minima in boundary energy. Among them, four configurations with relatively low boundary energies are shown in Fig. 4. In accordance with the figures, these will be noted as configurations A–D hereafter. The configurations contain some atoms that have threefold and fivefold coordination of the first-nearest neighbors in contrast to the fourfold coordination in wurtzite structure. Such atoms are marked with asterisks in the respective figures. The figures also display simulated HRTEM images based on these models in comparison with an enlargement of the HRTEM image of the 20° boundary shown in Fig. 2(c). Additionally, the calculated boundary energies are listed along with the number of threefold- and fivefold-coordinated atoms per unit interfacial area in Table II. These energies were obtained for the supercells containing 292–304 atoms, while smaller supercells composed of 180–192 atoms gave larger energies by 8% for the configuration A and 1% for the configurations B–D. It is therefore considered that the values listed in the tables converge well with respect to the boundary separation, and the four configurations have similar boundary energies within the approximation used in the present calculation. In our previous study on the same $\Sigma=7$ boundary, two other atomic configurations have been modeled with comparable boundary energies.¹⁴ However, these configurations were not investigated in the present study because of the largely asymmetric core structures in contrast to the experimental image.

It is recognized that the local atomic arrangements are significantly different between the four configurations despite the similarity in energy. The configuration A was obtained in a $[0001]$ translation state with an amount of half the lattice constant c . A large open channel is present at the boundary core, and this includes four atoms that are missing one of the four first-nearest neighbors as marked with asterisks. The configuration B also has four threefold-coordinated atoms per periodicity unit. However, this does not include a translation in the $[0001]$ direction, and the structure is mirror symmetric. In this configuration, there is also a large open channel, which can be represented by a connection of fivefold- and sevenfold-coordinated channels. The lattice is somewhat bent around this channel, particularly at the threefold-coordinated atoms. This can be attributed to a repulsive interaction between the atoms (ions) of like sign located close across the interface. A similar mirror symmetric structure is found in the configuration C. This configuration was obtained by adding one atomic column in the periodicity unit of the configuration B. As a result, only a small open channel coordinated by eight atomic columns has been left at

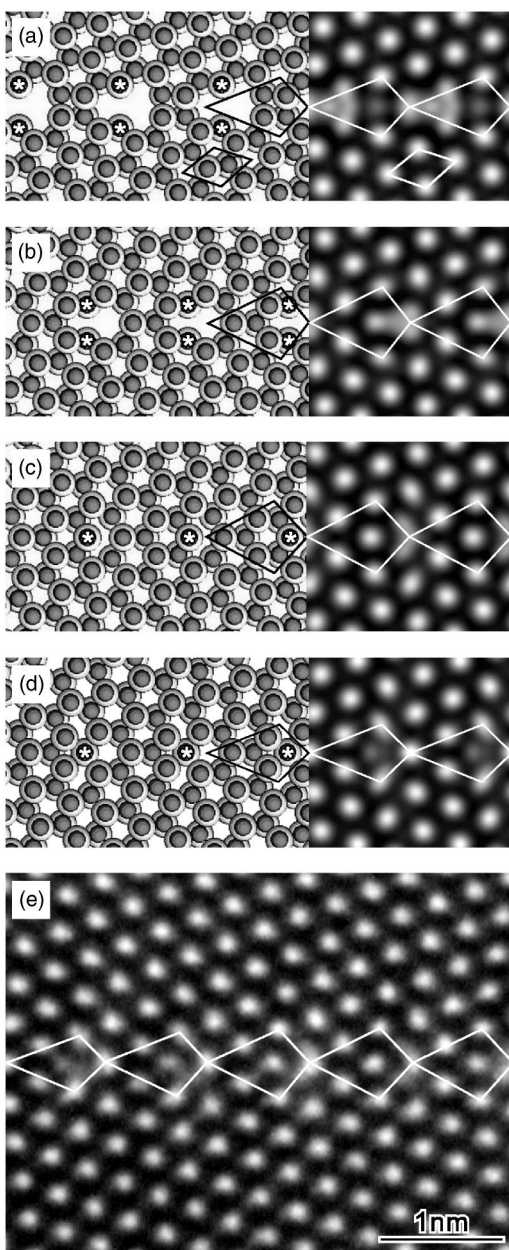


FIG. 4. (a)–(d) Atomic configurations of the $\{12\bar{3}0\}$ $\Sigma=7$ boundary modeled by atomistic calculations, A–D, along with corresponding simulated HRTEM images. The smaller and larger circles denote Zn and O, respectively. Atoms coordinated by three or five first-nearest neighbors are marked with asterisks. The boundary core structural units are represented by quadrilaterals; the smaller quadrilaterals in the figure (a) indicate the primitive cell. (e) HRTEM image of a 20° near $\Sigma=7$ $\{12\bar{3}0\}$ symmetric tilt boundary, which corresponds to part of the image shown in Fig. 2(c).

the boundary core. In addition, the density of threefold-coordinated atoms has been reduced to half, without a significant enhancement of the lattice distortion. This may explain the lower boundary energy than that of the configuration B. The configuration D with a mirror symmetric structure was generated by removing one of the threefold-coordinated atomic columns from the configuration B. In the resultant atomic arrangement, there are no threefold-

TABLE II. Energies of atomic configurations of the $\{12\bar{3}0\}$ $\Sigma=7$ boundary obtained by atomistic calculations. Number of threefold- or fivefold-coordinated atoms per unit boundary area is also shown along with the coordination number (in parentheses).

Configuration	Energy (Jm^{-2})	Number of threefold- or fivefold-coordinated atoms per unit boundary area (coordination number)
A	1.47	4 (3)
B	1.69	4 (3)
C	1.54	2 (3)
D	1.54	2 (5)

coordinated atoms but some atoms have five first-nearest neighbors. These atoms form a fourfold-coordinated channel at the boundary core, in contrast to the sixfold-coordinated channels in the bulk regions. Around the fourfold-coordinated channels, atoms (ions) of like sign are very close to each other. This may be a reason why the boundary energy is comparable to those of the other configurations despite the absence of threefold-coordinated atoms.

HRTEM image simulations were conducted using the four atomic configurations with a defocus and a specimen thickness varied. The results indicated that the configurations B–D with a specimen thickness of 5 nm and a defocus of -26 nm give the best agreement with the experimental image shown in Fig. 4(e) as discussed below. The simulated images shown in Figs. 4(a)–4(d) were obtained under this condition, where atomic columns located parallel to the $[0001]$ direction appear dark and the bright spots approximately represent open channels. The latter corresponds to the corners of the ZnO primitive cell as indicated in Fig. 4(a).

The experimental image shown in Fig. 4(e) has a periodic and nearly mirror symmetric character as clarified by drawings of the structural units along $\{10\bar{1}0\}$ planes. In detail, it seems to include a variation in the shape of the units. The third to fifth units from the left look wider than the first and second ones in the direction of the boundary normal, and show somewhat different image features. In accordance with the experimental image, the simulated images for the modeled configurations have a symmetric character. However, the configuration A shows a T-shaped bright spot associated with a large open channel at a left half of the unit, in contrast to the experimental image. This tendency was also found in the simulated images obtained under other conditions. The configuration A can therefore be ruled out from the candidates. Concerning the configuration B, a notable feature is that the bright spot located inside the unit is connected to a vertically elongated spot at the right-hand edge of the unit. It is also T shaped, but is much smaller than that in the configuration A. This can be attributed to such a shape of the open channel in the boundary atomic configuration shown in the left figure. On the other hand, the spot inside the unit is clearly separated from the one at the right-hand edge in the configuration C. Moreover, the latter is significantly stretched to be U shaped. These features were not recognized in the configuration B under any image simulation condi-

tions. The configuration D shows a narrower unit in the direction of the boundary normal. The bright spot inside the unit is relatively weak, which should be due to a small open channel surrounded only by four atomic columns as recognized in the left figure. In addition, the spots located at the upper and lower edges of the unit are elongated toward one of the neighboring spots.

Considering above-mentioned features in the simulated images, the first and second structural units from the left in the experimental image shown in Fig. 4(e) can be assigned to the configuration D, the third and fourth units to the configuration C, and the fifth unit to the configuration B or C. It seems that this near $\Sigma=7$ boundary has multiple structural units. Such configurations, particularly the configurations C and D, were also recognized in the other areas of the same boundary and at different boundaries with similar rotation angles. As shown in Table II, the configurations B and C have four and two threefold-coordinated atoms per unit boundary area, 0.45 nm^{-2} , respectively. The presence of these configurations indicates that a high density of dangling bonds has been left along the boundary cores rather than reconstructed as in the case of the configuration D.

For GaN that also has wurtzite structure, very similar periodicity units of the $\Sigma=7$ boundary have been reported.^{29,57,58} Potin *et al.* have conducted extensive investigation of edge dislocations and [0001]-tilt grain boundaries in GaN using HRTEM and anisotropic elasticity calculations. They suggested that three types of core structures are present in edge dislocations, and many of the low Σ tilt boundaries, including the $\Sigma=7$ can be described as an array of these dislocations.²⁹ Such boundary atomic configurations in GaN have also been modeled through empirical atomistic calculations by Béré and Serra⁵⁷ and by Chen *et al.*⁵⁸ It appears that the structural units of [0001]-tilt boundaries in ZnO have a similar character, as discussed in the next section.

C. Relationship between core structures of [0001]-tilt boundaries and edge dislocations

Figure 5 shows typical HRTEM images of isolated edge dislocations with drawings of their core structural units. These dislocations were located in the same grain with a separation of about 30 nm, and therefore the local TEM foil thicknesses are expected to be similar. Additionally, a defocus employed for these images is close to that for the image of the $\Sigma=7$ boundary shown in Fig. 4(e). The Burgers circuits, which are made on the basis of bright spots representing the primitive cell edges, indicate that the dislocations have an edge component with $\mathbf{b}=1/3\langle 11\bar{2}0 \rangle$. A screw component is likely to be absent at these dislocations since no anisotropic contrast was observed with an incident beam tilted. It is interesting that image features at the dislocation cores look very similar to those at the 20° near $\Sigma=7$ boundary given in the Fig. 4(e). For the dislocation shown in Fig. 5(a), a U-shaped bright spot is recognized at the right-hand edge of the core structural unit. This suggests that the atomic configuration is similar to the modeled configuration C of the $\Sigma=7$ boundary, where an eightfold-coordinated channel is present. On the other hand, the core unit of the dislocation

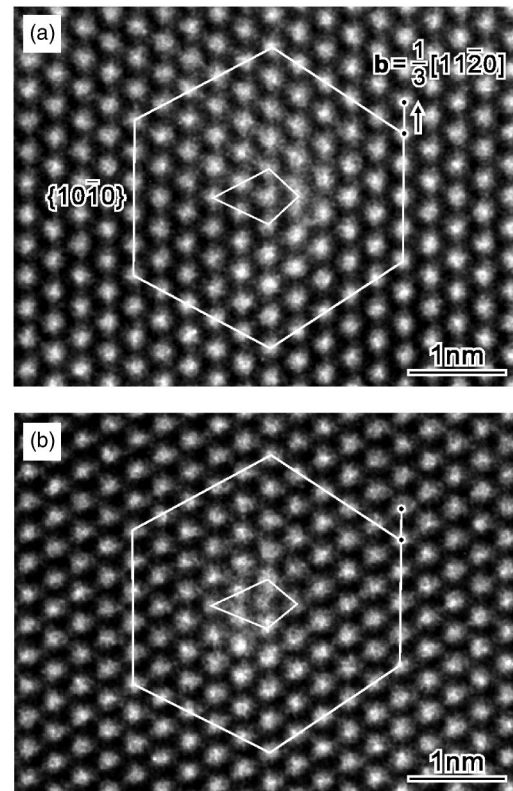


FIG. 5. HRTEM images of typical isolated edge dislocations. Burgers circuits and core structural units are drawn along $\{10\bar{1}0\}$ planes.

shown in Fig. 5(b) comprises a relatively weak bright spot near the center and elongated spots at the upper and lower edges. These characters agree with the modeled configuration D with a fourfold-coordinated channel.

HRTEM observation was conducted for more than 15 isolated edge dislocations with $\mathbf{b}=1/3\langle 11\bar{2}0 \rangle$. Three of them looked very similar to the one shown in Fig. 5(b), indicative of the atomic configuration corresponding to the configuration D of the $\Sigma=7$. The others were basically assigned to the configuration C, but some of them showed features between the configurations B and C and may correspond to the configuration B. The atomistic calculations conducted for the $\Sigma=7$ boundary suggested that the configuration B with fivefold and sevenfold-coordinated channels shows a somewhat higher energy than the configurations C and D with eightfold- and fourfold-coordinated channels. This may hold for dislocations likewise and explain why the configurations C and D were more frequently observed in the present ZnO thin film.

The core structure of $1/3\langle 11\bar{2}0 \rangle$ edge dislocations in GaN has been investigated in detail through HR-TEM and -STEM observations and first-principles and empirical calculations.^{29,59-62} Potin *et al.* have reported that fivefold and sevenfold-coordination and eightfold-coordination core structures were observed at the edge dislocations in GaN with a similar frequency, while configurations with fourfold-coordinated channels were not found.²⁹ Béré and Serra have shown through atomistic calculations that the eightfold and

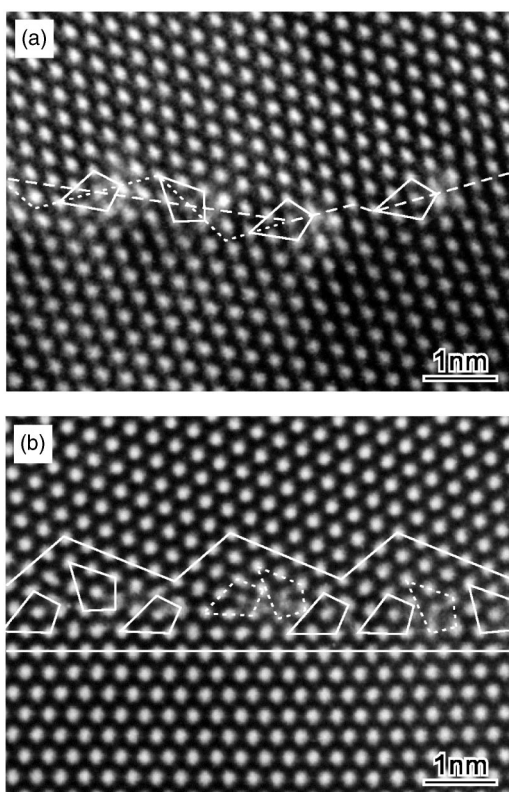


FIG. 6. Enlargements of part of the HRTEM images shown in Fig. 2. (a) 10.6° boundary with a drawing of dislocationlike structural units (solid) and approximate local boundary planes in two ways (broken). (b) 20.1° boundary with a $\{10\bar{1}0\}$ facet structure. The boundary plane and periodicity are approximately shown by lines along $\{10\bar{1}0\}$ planes as well as dislocationlike units.

fourfold configurations are correlated with each other by glide of the dislocations, and both are connected with the fivefold-sevenfold configuration by climb.⁶¹ The eightfold and fourfold configurations are similar in energy, while the fivefold-sevenfold configuration is somewhat lower.⁶¹ Atomistic calculations done by Chen *et al.* also show that the fivefold-sevenfold configuration has the lowest energy among the three configurations.⁶² In GaN, Ga-Ga and N-N bonding interactions are possible in addition to Ga-N bonding because of a covalent nature.⁶¹ The fivefold-sevenfold configuration, where the same species are forced to be close to each other, may therefore be relatively favorable, compared to ZnO with more ionicity. Although a further experimental-theoretical study should be required to draw a conclusion on the dominant configurations of the edge dislocations in ZnO, it can be concluded that there are multiple dislocation core structures that are closely related to the structural units of the $\Sigma=7$ boundaries. It seems that other boundaries have similar local atomic structures as discussed below.

Figure 6 displays enlargements of part of the boundaries shown in Figs. 2(a) and 2(b) with drawings of edge dislocationlike units along $\{10\bar{1}0\}$ planes. The images have been flipped horizontally so that the directions of the units are close to those at the $\Sigma=7$ boundary and the edge dislocations

shown in Figs. 4 and 5. It is found that the 10.6° boundary shown in Fig. 6(a) comprises a series of dislocationlike units. Image features of these units look similar to the ones recognized at the dislocation given in Fig. 5(a) and therefore to the configuration C with an eightfold-coordinated channel. The dislocation array is not regular, and interestingly, the second dislocation from the left has a Burgers vector that makes an angle of about 60° with the others. This character can be generally explained in terms of the orientation of local boundary planes. When a local boundary plane makes a low angle with respect to one of the $\{11\bar{2}0\}$ planes, i.e., the boundary normal is close to the direction of the Burgers vector, the misorientation can be readily accommodated by dislocations with a Burgers vector nearly perpendicular to the boundary. The right half of the low-angle boundary shown in Fig. 6(a) can be categorized into this case, where a local boundary plane is relatively close to $\{11\bar{2}0\}$, as represented by a broken line. On the other hand, a zigzag array comprising the two types of dislocations is required to form a macroscopic boundary plane close to one of the $\{10\bar{1}0\}$ planes, since its normal makes 30° with the Burgers vectors. The left half of the boundary shown in Fig. 6(a) is regarded as an example of this kind if we assume, for instance, a macroscopic boundary plane located on the coarser broken line. Alternatively, it is considered from a more microscopic viewpoint that this part consists of small facets or steps that have local boundary planes identical or crystallographically equivalent to the right half. This is approximately represented by the finer broken line in Fig. 6(a).

The 20.1° asymmetric boundary shown in Fig. 6(b) is also composed of dislocations with two types of the Burgers vector directions. These dislocations look similar to the configuration C with an eightfold-coordinated channel although the assignment is somewhat ambiguous, particularly for the units drawn with broken lines. The boundary plane is located near one of $\{10\bar{1}0\}$ planes of the lower grain as clarified by a straight line. A zigzag arrangement of dislocationlike units forms this boundary plane, which is consistent with the above discussion. Since this misorientation is close to the $\Sigma=7$, the boundary plane also corresponds approximately to one of $\{35\bar{8}0\}$ planes of the upper grain. This boundary, therefore, has a possibility to exhibit a periodicity associated with this plane as indicated by a drawing. Atomistic calculations reported on the asymmetric $\Sigma=7$ boundary in GaN show that a periodicity unit is formed by a zigzag array of three dislocationlike units where two are inclined toward the grain having a $(10\bar{1}0)$ boundary plane and one is toward the other grain.⁵⁷ The first and second periodicity units from the left at the present boundary may have a similar character although the structure inside the units is not regular. The imperfectness in the periodicity units may be attributed to a 1.7° deviation in rotation angle from the exact $\Sigma=7$. It has been reported that the asymmetric $\Sigma=7$ boundary with almost no angle deviation in GaN has a very flat $(10\bar{1}0)$ structure with a regular periodicity unit, where fourfold-coordinated channels are also present as in the case of the configuration D modeled in the present study.²⁹ On the other hand, Kiselev *et al.* have shown that a $(10\bar{1}0)$ $\Sigma=31$ asym-

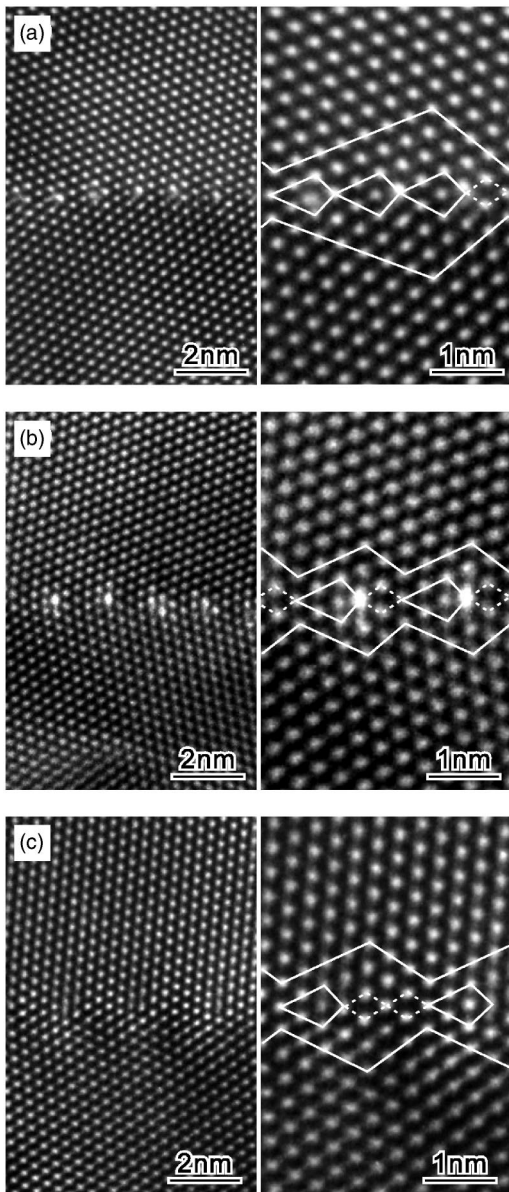


FIG. 7. HRTEM images of boundaries nearly in low Σ CSL misorientations where the lowest angles made by the $\{11\bar{2}0\}$ planes of the upper and lower grains are equal to the rotation angles. (a) $18.9 \pm 0.1^\circ$ near $\{4\ 7\ 11\ 0\}$ $\Sigma=31$ boundary. (b) $13.8 \pm 0.2^\circ$ near $\Sigma=19$ $\{23\bar{5}0\}$ boundary. (c) $10.4 \pm 0.2^\circ$ near $\Sigma=37$ $\{34\bar{7}0\}$ boundary. The right figures show enlargements of part of the left figures. The ideal periodicity units are drawn along $\{10\bar{1}0\}$ planes as well as dislocationlike units (solid) and bulklike units (broken).

metric boundary in a ZnO bicrystal comprises small $(10\bar{1}0)$ facets rather than a large flat $(10\bar{1}0)$ boundary plane, despite the nearly exact misorientation.¹⁹

Core structures described as a linkage of dislocationlike structural units were also found at other boundaries in the present thin films. Figures 7 and 8 display HRTEM images of boundaries nearly in low Σ CSL misorientations with symmetric structures. For the boundaries shown in Fig. 7, the lowest angles made by the $\{11\bar{2}0\}$ planes of the upper and

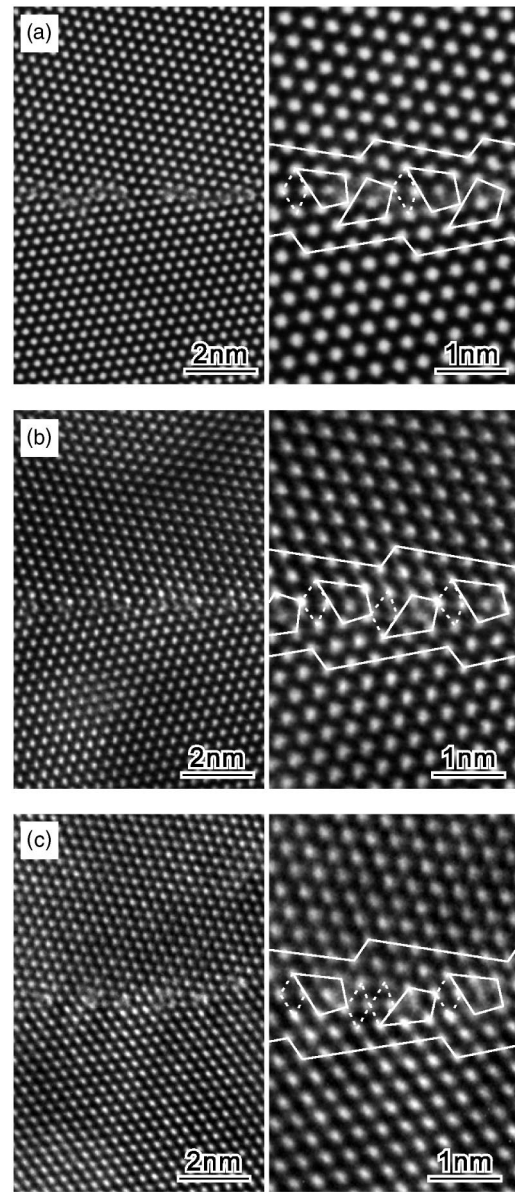


FIG. 8. HRTEM images of boundaries nearly in low Σ CSL misorientations where the lowest angles made by the $\{10\bar{1}0\}$ planes of the upper and lower grains are equal to the rotation angles. (a) $20.1 \pm 0.2^\circ$ near $\Sigma=7$ $\{14\bar{5}0\}$ boundary. (b) $18.9 \pm 0.1^\circ$ near $\Sigma=31$ $\{15\bar{6}0\}$ boundary. (c) $14.9 \pm 0.4^\circ$ near $\Sigma=43$ $\{16\bar{7}0\}$ boundary. The right figures show enlargements of part of the left figures. The ideal periodicity units are drawn along $\{10\bar{1}0\}$ planes as well as dislocationlike units (solid) and bulklike units (broken).

lower grains are equal to the rotation angles. The boundary planes are located almost in the middle of them and therefore closer to one of the $\{11\bar{2}0\}$ planes than any of the $\{10\bar{1}0\}$ planes. It is found in the right figures that all the boundaries have dislocationlike structural units, and the dislocations with the same Burgers vectors are aligned almost straightly, consistent with the above discussion. Most of the structural units at these boundaries have image features similar to the configuration B or C, but the detailed assignment is rather difficult from these images. Apart from distortion, the ar-

rangement of the bright spots between the dislocationlike units is similar to the bulk region. The combination of these dislocationlike and bulklike units constructs periodicity units particular to respective Σ values and boundary planes. This is schematically shown in Fig. 9 for the exact CSL misorientations. As illustrated in Fig. 9(a), to the left, a vector of $1/3[4\bar{5}10]$ can represent the periodicity and a $(21\bar{3}0)$ boundary plane of the $\{12\bar{3}0\}$ $\Sigma=7$ boundary. The circuit drawn in right figure indicates that this periodicity unit corresponds to the $1/3(11\bar{2}0)$ edge dislocation. The other boundary planes can be described as a straight array of the $\Sigma=7$ dislocationlike units and the bulklike units. Accordingly, as the rotation angle decreases from the $\Sigma=31$ in Figs. 7(a) and 9(b) to the $\Sigma=37$ in Figs. 7(c) and 9(d), the bulklike regions become wider as in the case of the so-called low-angle boundaries. On the other hand, the periodicity units cannot be represented by a straight arrangement of the dislocationlike and bulklike units under some misorientations. One example is the $\{25\bar{7}0\}$ $\Sigma=13$ boundary given in Fig. 9(e). In this case, a shift of the dislocationlike units may complete the periodicity unit, as shown in the lower figure. This model looks similar to the structure of a $\{25\bar{7}0\}$ $\Sigma=13$ boundary observed in a ZnO bicrystal by Kiselev *et al.*¹⁹ and that simulated for GaN by Béré and Serra.⁵⁷ Thus, this type of symmetric boundary in ZnO may comprise an array of dislocationlike and bulklike units. When a misorientation is represented by a straight array of these units, the atomic arrangement at the boundary can be purely symmetric in view of the symmetric nature of the structural units. On the other hand, the arrangement should be locally asymmetric under some misorientations where a shift of the structural units is required as in the case of the $\Sigma=13$ boundary.

The boundaries displayed in Fig. 8 look somewhat different from those given in Fig. 7. At these boundaries, the low-angle angles made by the $\{10\bar{1}0\}$ planes of the upper and lower grains are equal to the rotation angles. The boundary planes are located almost in the middle of them and therefore closer to one of the $\{10\bar{1}0\}$ planes than any of the $\{11\bar{2}0\}$ planes, in contrast to the boundaries shown in Fig. 7. The periodicity units are constructed by a zigzag array of dislocationlike units plus bulklike units, which should be associated with the boundary planes relatively close to one of $\{10\bar{1}0\}$, as mentioned above. In Fig. 10, the geometries of these boundaries are illustrated for the exact Σ misorientations. As shown in Fig. 10(a), a periodicity unit vector of the $\{14\bar{5}0\}$ $\Sigma=7$ boundary, the $[3\bar{2}10]$, can be represented by a combination of the $1/3[4\bar{5}10]$ and $1/3[5\bar{1}40]$ $\Sigma=7$ units. In other words, two dislocations whose Burgers vectors make 60° with each other constitute the periodicity unit. In detail, the near $\Sigma=7$ boundary given in Fig. 8(a) does not have such a simple periodicity unit but includes a shift of one of the dislocationlike units, as schematically shown in the lower part of Fig. 10(a). The near $\Sigma=31$ and 43 boundaries in Figs. 8(b) and 8(c) seem to have similar structural units. These geometries can be described as a pair of $1/3[4\bar{5}10]$ and $1/3[5\bar{1}40]$ $\Sigma=7$ units plus bulklike units, as illustrated in Figs. 10(b) and

10(c), where a shift of the units is not shown for simplicity. The number of bulklike units increases as the rotation angle decreases from the 21.79° ($\Sigma=7$) to 15.18° ($\Sigma=43$). On the other hand, there should be misorientations that cannot be described in this way. For instance, the $\{13\bar{4}0\}$ $\Sigma=13$ boundary has a shorter periodicity than the $\{14\bar{5}0\}$ $\Sigma=7$ boundary and it cannot be completed by the $1/3[4\bar{5}10]$ and $1/3[5\bar{1}40]$ $\Sigma=7$ units without an overlap as shown in the upper part of Fig. 10(d). In this case, the periodicity unit may include a shift of the units similar to the $\Sigma=7$, 31, and 43 boundaries to avoid an overlap, as shown in the lower figure. Actually, a structure similar to the latter has been observed at a $\{25\bar{7}0\}$ $\Sigma=13$ boundary in a ZnO bicrystal by Kiselev *et al.*¹⁹ and modeled using a combination of empirical and first-principles calculations by Carlsson *et al.*¹⁶ This type of boundary may thus be generally represented by a zigzag array of dislocationlike units plus bulklike units. The image area in Fig. 8(a) corresponds to a symmetric part of the 20.1° near $\Sigma=7$ boundary given in Fig. 2(b) and is therefore adjacent to the $\{10\bar{1}0\}$ facet structure shown in Fig. 6(b). These two structures are smoothly connected through a shift of dislocationlike units at this boundary. Such a transition is also found at the right-hand side of the $\Sigma=43$ boundary in the left of Fig. 8(c), where a symmetric structure was observed at a very small area compared to the other boundaries. The dislocations may be easily rearranged to shift local $\{10\bar{1}0\}$ boundary plane in a structural unit with a large periodicity.

At the boundaries shown in Figs. 7 and 8, the interval of dislocation units is not perfectly regular in the whole of the boundary areas, which may be attributed to the deviations of 0.3° – 1.7° from the exact CSL misorientations illustrated in Figs. 9 and 10. Nevertheless, the boundaries are nearly symmetric in relatively wide areas. This may be due to the tendency that the boundary structural units are composed of edge dislocations. In this case, dislocations can be readily shifted to accommodate the deviation in rotation angle from the exact low Σ CSL misorientations, without significantly disturbing the symmetry with respect to boundary planes. Such shift of the dislocationlike structural units can be interpreted on the basis of the displacement shift complete.^{29,63} Alternatively, the geometries with angle deviations from those of the exact low Σ correspond to the CSL misorientations with high Σ values ($\Sigma > 50$), which in turn implies that such high Σ boundaries are represented by similar structural units. It appears that many of [0001]-tilt boundaries can have nearly symmetric structures composed of dislocationlike structural units even if there are some angle deviations from the highly coincident geometries. In practice, not limited to the boundaries shown in Figs. 7 and 8, nearly symmetric structures were frequently observed in the present thin film when the rotation angles were not very low (roughly speaking, higher than 10°). The symmetric structures, i.e., the straight or regular zigzag arrangements of dislocations, may be energetically preferable, compared to the others, such as irregular dislocation array and $\{10\bar{1}0\}$ facet structures.

The [0001]-tilt boundaries in ZnO can thus be generally described as an array of dislocationlike structural units. Such atomic structures are very similar to those reported for

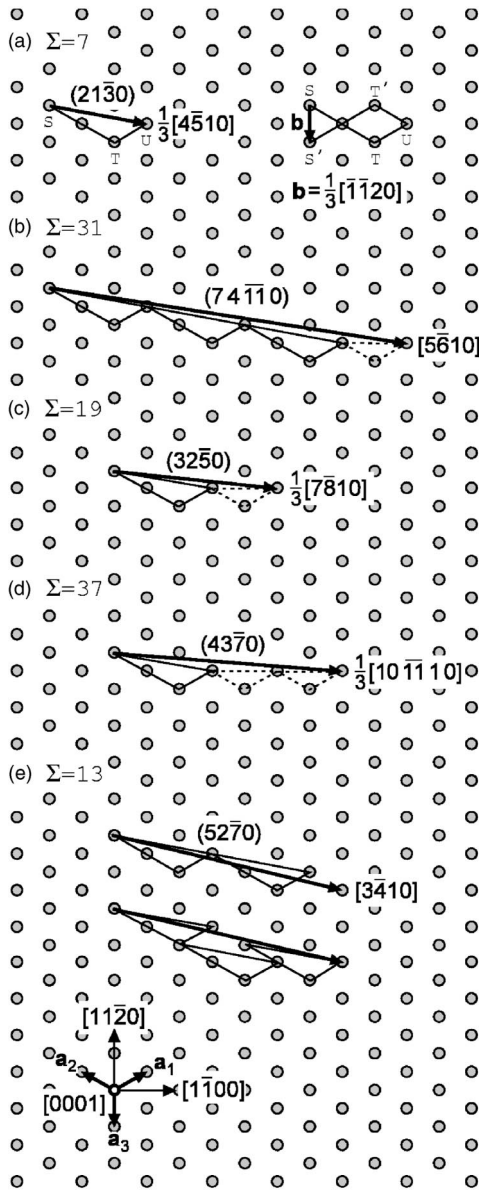


FIG. 9. Schematics showing symmetric periodicity units for boundaries in low Σ CSL misorientations where the boundary planes make angles of $\theta/2$ with the $(11\bar{2}0)$ plane and the $[1\bar{1}00]$ direction (θ : rotation angle). The filled circles denote open channels or the primitive cell edges in the $[0001]$ view of the wurtzite structure. \mathbf{a}_1 – \mathbf{a}_3 correspond to three of $1/3\langle 11\bar{2}0 \rangle$ primitive translation vectors. (a) $\Sigma=7$ ($\theta=21.79^\circ$). The periodicity unit is drawn for half the unit associated with the lower grain. The bold arrow indicates the periodicity unit vector of $1/3[4\bar{5}10]$ and the corresponding boundary plane of $(21\bar{3}0)$. The circuit S-T-U-T'-S' in the right represents the full unit, showing that this unit corresponds to an edge dislocation with a Burgers vector of $1/3[1\bar{1}20]$. (b)–(d) $\Sigma=31$ ($\theta=17.90^\circ$), $\Sigma=19$ ($\theta=13.17^\circ$), and $\Sigma=37$ ($\theta=9.43^\circ$). The boundaries displayed in Fig. 7 are nearly in these misorientations. Periodicity unit vectors and corresponding boundary planes (bold) are described as a combination of the $1/3[4\bar{5}10]\Sigma=7$ units (solid) and bulklike units (broken). (e) $\Sigma=13$ ($\theta=27.80^\circ$). An incomplete unit formed by two $\Sigma=7$ units (upper) and a complete unit including a shift of the $\Sigma=7$ units (lower).

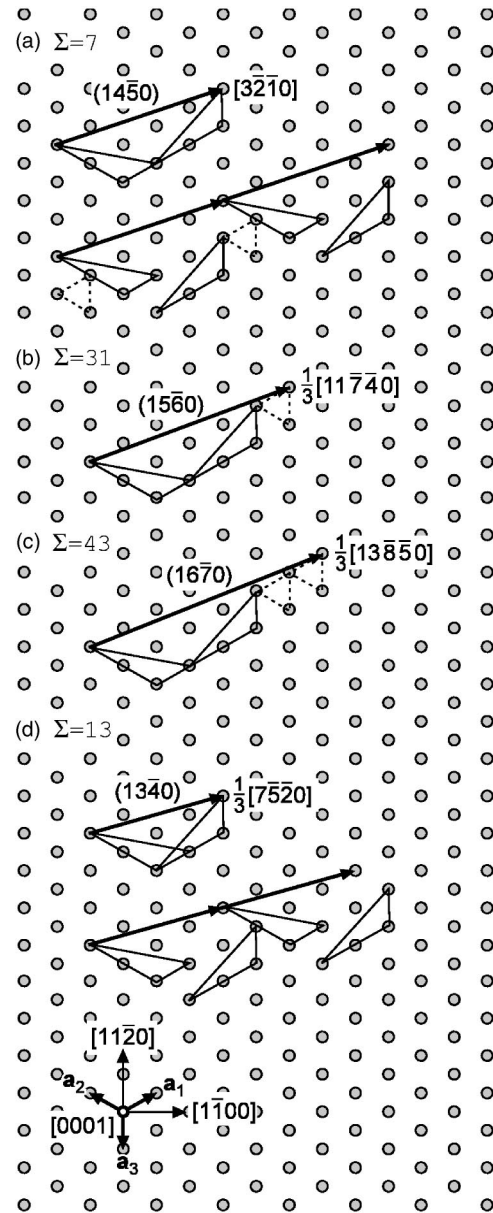


FIG. 10. Schematics showing symmetric periodicity units for boundaries in low Σ CSL misorientations where the boundary planes make angles of $(60^\circ - \theta)/2$ with the $(11\bar{2}0)$ plane and the $[1\bar{1}00]$ direction (θ : rotation angle). The corresponding angles with the $(01\bar{1}0)$ plane and the $[2\bar{1}\bar{1}0]$ direction that are parallel to \mathbf{a}_1 are equal to $\theta/2$ (\mathbf{a}_1 – \mathbf{a}_3 : three of $1/3\langle 11\bar{2}0 \rangle$ primitive translation vectors). The filled circles denote open channels or the primitive cell edges in the $[0001]$ view of the wurtzite structure. (a)–(c) $\Sigma=7$ ($\theta=21.79^\circ$), $\Sigma=31$ ($\theta=17.90^\circ$), and $\Sigma=43$ ($\theta=15.18^\circ$). The boundaries displayed in Fig. 8 are nearly in these misorientations. (d) $\Sigma=13$ ($\theta=27.80^\circ$). Periodicity unit vectors and corresponding boundary planes are described as a pair of $1/3[4\bar{5}10]$ $\Sigma=7$ units (solid) and bulklike units (broken). The lower figures in (a) and (d) denote periodicity unit models that include a shift of the $\Sigma=7$ units.

GaN,^{29,57,58} despite a difference in ionicity and covalency. This may indicate that the structure of [0001]-tilt boundaries in the wurtzite system is mainly determined by geometric and symmetric constraints. Further systematic experimental and theoretical studies including other hexagonal systems will clarify the generality and specialty of the boundary structures.

IV. CONCLUSIONS

HRTEM observation was conducted for [0001]-tilt grain boundaries in fiber-textured ZnO thin films to investigate their atomic structures. Three types of boundaries were observed: low-angle boundaries described as an irregular array of dislocations, boundaries with $\{10\bar{1}0\}$ facet structures, and near-low Σ boundaries with symmetric structural units. The atomistic calculations combined with HRTEM image simulations for a $\Sigma=7$ boundary indicated the presence of mul-

tipple structure units that are very similar to edge dislocation cores. Not only low-angle boundaries, but also high-angle boundaries with nearly symmetric and $\{10\bar{1}0\}$ facet structures are composed of the dislocationlike structural units. The structural units are arranged straightly or in a zigzag to accommodate the rotation angles, depending on boundary planes. The present results suggest that [0001]-tilt boundaries in ZnO are generally described as an array of the dislocationlike units.

ACKNOWLEDGMENTS

We thank Dr. J. D. Gale for allowing us to use the GULP program code. This work was supported by a Grant in Aid for Scientific Research and Special Coordination Funds from the Ministry of Education, Culture, Sports, Science and Technology of Japan. F.O. also thanks the Japan Society for the Promotion of Science for the research fellowship.

*Present address: Department of Materials Science and Engineering, Kyoto University, Yoshida-Honmachi, Sakyo-ku, Kyoto 606-8501, Japan. Electronic address: fumiyasu.oba@materials.mbox.media.kyoto-u.ac.jp

†Electronic address: ikuhara@sigma.t.u-tokyo.ac.jp

¹O. L. Krivanek, S. Isoda, and K. Kobayashi, *Philos. Mag.* **36**, 931 (1977).

²J. M. Penisson and A. Bourret, *Philos. Mag. A* **40**, 811 (1979).

³K. L. Merkle and D. J. Smith, *Phys. Rev. Lett.* **59**, 2887 (1987).

⁴F. Ernst, M. W. Finnis, D. Hofmann, T. Muschik, U. Schönberger, U. Wolf, and M. Methfessel, *Phys. Rev. Lett.* **69**, 620 (1992).

⁵M. M. McGibbon, N. D. Browning, M. F. Chisholm, A. J. McGibbon, S. J. Pennycook, V. Ravikumar, and V. P. Dravid, *Science* **266**, 102 (1994).

⁶N. D. Browning, J. P. Buban, H. O. Moltaji, S. J. Pennycook, G. Duscher, K. D. Johnson, R. P. Rodrigues, and V. P. Dravid, *Appl. Phys. Lett.* **74**, 2638 (1999).

⁷D. M. Duffy and P. W. Tasker, *Philos. Mag. A* **47**, 817 (1983).

⁸D. Wolf, *J. Am. Ceram. Soc.* **67**, 1 (1984).

⁹J. D. Rittner and D. N. Seidman, *Phys. Rev. B* **54**, 6999 (1996).

¹⁰M. Kohyama, *Modell. Simul. Mater. Sci. Eng.* **10**, R31 (2002).

¹¹I. Dawson, P. D. Bristowe, M. H. Lee, M. C. Payne, M. D. Segall, and J. A. White, *Phys. Rev. B* **54**, 13 727 (1996).

¹²S. D. Mo, W. Y. Ching, M. F. Chisholm, and G. Duscher, *Phys. Rev. B* **60**, 2416 (1999).

¹³S. Fabris and C. Elsässer, *Phys. Rev. B* **64**, 245117 (2001).

¹⁴F. Oba, I. Tanaka, S. R. Nishitani, H. Adachi, B. Slater, and D. H. Gay, *Philos. Mag. A* **80**, 1567 (2000).

¹⁵F. Oba, S. R. Nishitani, H. Adachi, I. Tanaka, M. Kohyama, and S. Tanaka, *Phys. Rev. B* **63**, 045410 (2001).

¹⁶J. M. Carlsson, B. Hellsing, H. S. Domingos, and P. D. Bristowe, *J. Phys.: Condens. Matter* **13**, 9937 (2001).

¹⁷T. Höche, P. R. Kenway, H.-J. Kleebe, M. Rühle, and P. A. Morris, *J. Am. Ceram. Soc.* **77**, 339 (1994).

¹⁸U. Dahmen, S. Paciornik, I. G. Solorzano, and J. B. Vandersande, *Interface Sci.* **2**, 125 (1994).

¹⁹N. Kiselev, F. Sarrazit, E. A. Stepantsov, E. Olsson, T. Claeson,

V. I. Bondarenko, R. C. Pond, and N. A. Kiselev, *Philos. Mag. A* **76**, 633 (1997).

²⁰Y. Ikuhara, T. Watanabe, T. Saito, H. Yoshida, and T. Sakuma, *Mater. Sci. Forum* **284–286**, 273 (1999).

²¹T. Yamamoto, K. Hayashi, Y. Ikuhara, and T. Sakuma, *J. Am. Ceram. Soc.* **83**, 1527 (2000).

²²E. C. Dickey, X. D. Fan, and S. J. Pennycook, *J. Am. Ceram. Soc.* **84**, 1361 (2001).

²³S. Nufer, A. G. Marinopoulos, T. Gemming, C. Elsässer, W. Kurtz, S. Köstlmeier, and M. Rühle, *Phys. Rev. Lett.* **86**, 5066 (2001).

²⁴N. Shibata, F. Oba, T. Yamamoto, Y. Ikuhara, and T. Sakuma, *Philos. Mag. Lett.* **82**, 393 (2002).

²⁵Z. Zhang, W. Sigle, and M. Rühle, *Phys. Rev. B* **66**, 094108 (2002).

²⁶H. Nishimura, K. Matsunaga, T. Saito, T. Yamamoto, and Y. Ikuhara, *J. Am. Ceram. Soc.* **86**, 574 (2003).

²⁷N. Shibata, F. Oba, T. Yamamoto, T. Sakuma, and Y. Ikuhara, *Philos. Mag.* **83**, 2221 (2003).

²⁸K. L. Merkle, G.-R. Bai, Z. Li, C.-Y. Song, and L. J. Thompson, *Phys. Status Solidi A* **166**, 73 (1998).

²⁹V. Potin, P. Ruterana, G. Nouet, R. C. Pond, and H. Morkoç, *Phys. Rev. B* **61**, 5587 (2000).

³⁰D. R. Clarke, *J. Am. Ceram. Soc.* **82**, 485 (1999).

³¹M. Matsuoka, *Jpn. J. Appl. Phys.* **10**, 736 (1971).

³²K. Mukae, K. Tsuda and I. Nagasawa, *Jpn. J. Appl. Phys.* **16**, 1361 (1977).

³³G. E. Pike and C. H. Seager, *J. Appl. Phys.* **50**, 3414 (1979).

³⁴F. Greuter, G. Blatter, M. Rossinelli, and F. Stucki, *Conduction Mechanism in ZnO-Varistors: An Overview*, in *Ceramic Transactions, Vol. 3, Advances in Varistor Technology*, edited by L. M. Levinson (American Ceramic Society, Westerville, OH, 1989), pp. 31–53

³⁵E. Olsson and G. L. Dunlop, *J. Appl. Phys.* **66**, 3666 (1989).

³⁶F. Stucki and F. Greuter, *Appl. Phys. Lett.* **57**, 446 (1990).

³⁷A. Tanaka and K. Mukae, *J. Electroceram.* **4:S1**, 55 (1999).

³⁸N. Ohashi, Y. Terada, T. Ohgaki, S. Tanaka, T. Tsurumi, O. Fuku-

- naga, H. Haneda, and J. Tanaka, *Jpn. J. Appl. Phys., Part 1* **38**, 5028 (1999).
- ³⁹Y. Sato, F. Oba, T. Yamamoto, Y. Ikuhara, and T. Sakuma, *J. Am. Ceram. Soc.* **85**, 2142 (2002).
- ⁴⁰F. Oba, Y. Sato, T. Yamamoto, Y. Ikuhara, and T. Sakuma, *J. Am. Ceram. Soc.* **86**, 1616 (2003).
- ⁴¹Y. Sato, F. Oba, M. Yodogawa, T. Yamamoto, and Y. Ikuhara, *J. Appl. Phys.* **95**, 1258 (2004).
- ⁴²M. A. McCoy, R. W. Grimes, and W. E. Lee, *J. Mater. Res.* **11**, 2009 (1996).
- ⁴³A. Rečnik, N. Daneu, T. Walther, and W. Mader, *J. Am. Ceram. Soc.* **84**, 2657 (2001).
- ⁴⁴P. Petrou, R. Singh, and D. E. Brodie, *Appl. Phys. Lett.* **35**, 930 (1979).
- ⁴⁵T. Minami, H. Nanto, and S. Takata, *Appl. Phys. Lett.* **41**, 958 (1982).
- ⁴⁶D. M. Bagnall, Y. F. Chen, Z. Zhu, T. Yao, S. Koyama, M. Y. Shen, and T. Goto, *Appl. Phys. Lett.* **70**, 2230 (1997).
- ⁴⁷H. Ohta, K. Kawamura, M. Orita, M. Hirano, N. Sarukura, and H. Hosono, *Appl. Phys. Lett.* **77**, 475 (2000).
- ⁴⁸D. G. Brandon, B. Ralph, S. Ranganathan and M. S. Wald, *Acta Metall.* **12**, 813 (1964).
- ⁴⁹J. D. Gale, *J. Chem. Soc., Faraday Trans.* **93**, 629 (1997).
- ⁵⁰G. V. Lewis and C. R. A. Catlow, *J. Phys. C* **18**, 1149 (1985).
- ⁵¹W. H. Press, S. A. Teukolsky, W. T. Vetterling, and B. P. Flannery, *Numerical Recipes*, 2nd ed. (Cambridge University Press, Cambridge, 1992), p. 418.
- ⁵²J. M. Cowley and A. F. Moodie, *Acta Crystallogr.* **10**, 609 (1957).
- ⁵³S. C. Abrahams and J. L. Bernstein, *Acta Crystallogr., Sect. B: Struct. Crystallogr. Cryst. Chem.* **25**, 1233 (1969).
- ⁵⁴A. P. Sutton and R. W. Balluffi, *Interfaces in Crystalline Materials* (Oxford University Press, New York, 1995), p. 20.
- ⁵⁵F. C. Frank, in *A Symposium on the Plastic Deformation of Crystalline Solids* (Office of Naval Research, Washington, DC, 1950), pp. 151.
- ⁵⁶J. P. Hirth and J. Lothe, *Theory of Dislocations*, 2nd Edition (Krieger, Melbourne, FL, 1982), p. 91.
- ⁵⁷A. Béré and A. Serra, *Phys. Rev. B* **66**, 085330 (2002).
- ⁵⁸J. Chen, P. Ruterana, and G. Nouet, *Phys. Rev. B* **67**, 205210 (2003).
- ⁵⁹Y. Xin, S. J. Pennycook, N. D. Browning, P. D. Nellist, S. Sivananthan, F. Omnès, B. Beaumont, J. P. Faurie, and P. Gibart, *Appl. Phys. Lett.* **72**, 2680 (1998).
- ⁶⁰J. Elsner, R. Jones, P. K. Sitch, V. D. Porezag, M. Elstner, Th. Frauenheim, M. I. Heggie, S. Öberg, and P. R. Briddon, *Phys. Rev. Lett.* **79**, 3672 (1997).
- ⁶¹A. Béré and A. Serra, *Phys. Rev. B* **65**, 205323 (2002).
- ⁶²J. Chen, P. Ruterana, and G. Nouet, *Mater. Sci. Eng., B* **B82**, 117 (2001).
- ⁶³W. Bollmann, *Crystal Defects and Crystalline Interfaces* (Springer, Berlin, 1970).